Molecular Dynamics Study on the Effect of Defects upon Shear Properties of Graphene

Akihiko Ito and Shingo Okamoto

***Abstract*—We investigated the shear properties of graphene containing point defects, such as vacancies, nitrogen atoms, and interlayer sp^3 carbons via molecular dynamics (MD) simulations. In the MD simulation, we used three types of potential functions: the second–generation reactive empirical bond order (REBO) potential for covalent C–C bonds, the Tersoff potential for covalent C–N bonds, and the Lennard-Jones potential for interlayer interactions in bilayer graphene. It was found that graphene is more sensitive to vacancy than sp^3 carbon or nitrogen atom unless these defects cluster in graphene.**

***Index Terms*—graphene, molecular dynamics, nitrogen, sp^3 carbon, shear strength**

I. Introduction

TODAY humankind faces crucial problems, such as the global warming and the exhaustion of fossil fuels. Carbon fibers are being investigated as potential candidates toward solving these problems owing to their superior mechanical and electrical properties. Graphene, which is basic structure in carbon fibers, have been found to have excellent tensile strength (~130 GPa) and the same Young's modulus (~1 TPa) as that of diamond. However the tensile strength of real carbon fibers is less than 5% of that of graphene. This decrease in the strength appears to be caused by various types of defects. Recently, many studies have been conducted on defects such as vacancies [1], [2], heteroatoms [3], sp^3-type defects [2], dislocations [4], and grain boundaries (GBs) [5] in carbon materials. Our goal is to clarify the relation between atomic-scale structures and mechanical properties of carbon fibers using molecular dynamics (MD) simulations. In the previous paper, we have clarified the tensile properties of graphene containing vacancies [6].

Carbon fibers derived from raw materials, such as polyacrylonitrile (PAN), pitch, and rayon, often contain impurities such as oxygen, nitrogen, or hydrogen atoms. Then these impurities may affect the mechanical and electronic properties of the carbon fibers. Recently, Shen *et al*. [7] investigated the effects of nitrogen (N) doping on the mechanical properties of ultrananocrystalline diamond (UNCD) films, using MD simulations. We performed the MD simulations on tensile loading of N-containing graphene in order to investigate the effect of N-atoms on tensile properties of graphene in our previous paper [8]. It was found that N-atoms had little effect on the tensile properties of graphene except when two nitrogen atoms adjoined each other in graphene. The tensile properties of bilayer graphene coupled by sp^3 carbons were investigated by Zhang *et al* using MD simulations [9]. The shear properties of pristine graphene were estimated by Min *et al* [10]. However, the shear properties of graphene with N-atoms and sp^3 carbons have not been clarified so far. In our previous work, we estimated the shear properties of graphene containing both N-atoms and vacancies, via MD simulations [11]. In addition, we clarified the shear properties of bilayer graphene containing both N-atoms and interlayer sp^3 carbons using MD simulations. In this study, we also clarified the effects of adjoining N-atoms on the shear properties of graphene.

Manuscript received May 10, 2014. This work was supported in part by the Ring-Ring project of JKA.

Akihiko Ito is with the Composite Materials Research Laboratories, Toray Industries, Inc., Masaki-cho 791-3193, Japan (e-mail: Akihiko_Ito@nts.toray.co.jp).

Shingo Okamoto is with the Graduate School of Science and Engineering, Ehime University, 3 Bunkyo-cho, Matsuyama 790-8577, Japan (e-mail: okamoto.shingo.mh@ehime-u.ac.jp).

II. Method

A. Potential Function

In the present study, we used three types of interatomic potentials: the second-generation reactive empirical bond order (2^{nd} REBO) [12], Tersoff [13], [14], and Lennard-Jones potentials. The 2^{nd} REBO potential for covalent C–C bonds is given by (1):

$$E_{REBO} = \sum_i \sum_{j>i} \left[V_R\left(r_{ij}\right) - B_{ij}^* V_A\left(r_{ij}\right) \right]. \quad (1)$$

The terms $V_R(r_{ij})$ and $V_A(r_{ij})$ denote the pair-additive interactions that reflect interatomic repulsions and attractions, respectively. The B_{ij}^* denotes the bond-order term.

The Tersoff potential for covalent C–N bonds is given by (2):

$$V = \frac{1}{2} \sum_{i \neq j} \left[f_C\left(r_{ij}\right) A_{ij} \exp\left(-\lambda_{ij} r_{ij}\right) - b_{ij} f_C\left(r_{ij}\right) B_{ij} \exp\left(-\mu_{ij} r_{ij}\right) \right], \quad (2)$$

where the parameter b_{ij} is the bond-order term that depends on the local environment.

$$b_{ij} = \chi_{ij}\left(1+\beta^{n_i}\zeta_{ij}^{n_i}\right)^{-1/2n_i} \quad (3)$$

$$\zeta_{ij} = \sum_{k\neq i,j} f_C(r_{ik})g(\theta_{ijk}) \quad , \quad (4)$$

$$g(\theta_{ijk}) = 1+\frac{c_i^2}{d_i^2}-\frac{c_i^2}{d_i^2+(h_i-\cos\theta_{ijk})^2} \quad , \quad (5)$$

where θ_{ijk} is the angle between bonds ij and ik.

The parameters A_{ij}, B_{ij}, λ_{ij}, and μ_{ij} depend on the atom type, namely, carbon or nitrogen. For atoms i and j (of different types), these parameters are

$$A_{ij} = \left(A_i \times A_j\right)^{\frac{1}{2}},\ B_{ij} = \left(B_i \times B_j\right)^{\frac{1}{2}} \quad (6)$$

$$\lambda_{ij} = \frac{\left(\lambda_i+\lambda_j\right)}{2},\ \mu_{ij} = \frac{\left(\mu_i+\mu_j\right)}{2} \quad , \quad (7)$$

where the parameters with a single index represent the interaction between atoms of the same type.

The parameter χ_{ij} in (3) takes into account the strengthening or weakening of the heteropolar bonds. There is no data for the determination of χ_{ij} for C–N interaction at present. In our model, this χ_{ij} is set to 0.8833 to obtain the lattice constants a and b of the graphitic-C_3N_4 orthorhombic structure as 4.10 and 4.70 Å, respectively similar to the previous work [8]. From discussions on the N–N interaction, we know that the N molecule does not interact with other atoms, because of its high binding energy (9.8 eV) and that it diffuses through the crystal and exits the surface. In our model, to keep the nitrogen molecule stable inside the crystalline structure, $\chi_{\text{N-N}}$ is set to zero [7], [14].

In this work, the cutoff length $R_{\min}$ in the cutoff function $f_C(r)$, given by (8) of both the 2nd REBO and the Tersoff potentials is set to 2.1 Å to avoid the dramatic increase in interatomic forces similar to the method in our previous paper [8].

$$f_c(r) = \begin{cases} 1, & r < R_{\min} \\ \left\{1+\cos\left[\dfrac{\pi(r-R_{\min})}{R_{\max}-R_{\min}}\right]\right\}/2, & R_{\min} < r < R_{\max} \\ 0, & r > R_{\max} \end{cases} . \quad (8)$$

The Lennard-Jones potential for the interlayer interaction in the bilayer graphene model is expressed as

$$V^{LJ} = 4\varepsilon\left[\left(\frac{r_0}{r_{ij}}\right)^{12}-\left(\frac{r_0}{r_{ij}}\right)^{6}\right]. \quad (9)$$

The 2nd REBO potential and the Lennard-Jones potential are switched according to the interatomic distance and bond order [15]. The value of ε is set to 0.00284 eV and r_0 is set to 3.2786 Å so that the interplanar spacing of graphite at 300 K is 3.35 Å, which is a known experimental value [16].

B. Analysis model

The analysis model of pristine graphene employed under the shear loading of armchair direction consists of 588 carbon atoms with dimensions identical to those of a real crystallite in typical carbon fibers [17], as shown in Fig. 1.

The analysis model of bilayer graphene under shear loading of armchair direction consists of 1,176 carbon atoms. That model is constructed by two layers of graphene sheet with the same size as the model shown in Fig. 1.

The example of graphene model containing randomly distributed vacancies and N-atoms under the shear loading is shown in Fig. 2. Vacancies were generated by randomly removing carbon atoms from the graphene model shown in Fig. 1. Then, N-atoms were generated by randomly replacing carbon atoms with nitrogen atoms. The positions of vacancies were set so that the vacancies could not cluster in graphene. The positions of N-atoms were also set in the same way. Three cases with constant vacancy-density of 4 % and differing N-contents, namely, 1 %, 2 %, and 4 %, were investigated. In addition, three cases with constant N-content of 4 % and differing vacancy-densities, namely, 1 %, 2 %, and 4 %, were investigated.

The example of bilayer graphene model containing randomly distributed interlayer sp^3 carbons and N-atoms under the shear loading is shown in Fig. 3. The interlayer sp^3 carbons were generated by vertically moving two atoms with the same plane coordinates (one in the upper layer and the other in the lower one) so that the distance between the two atoms could be 1.65 Å. Then, N-atoms were generated in the same way as the above mentioned one. Three cases with constant sp^3 carbon density of 5 % and differing N-contents, namely, 0 %, 1 %, and 4 %, were investigated. Furthermore, three cases with constant N-content of 4 % and differing sp^3 carbon densities, namely, 0 %, 1 %, and 5 %, were investigated. For references, three cases with constant N-content of 0 % and differing sp^3 carbon densities, namely, 0 %, 1 %, and 5 %, were investigated.

For all the models, the periodic boundary condition is imposed in only the Y direction in the calculations of shear loading. The analysis models consist of two parts. One part is referred to as the active zone, in which the atoms move according to their interactions with neighboring atoms. The

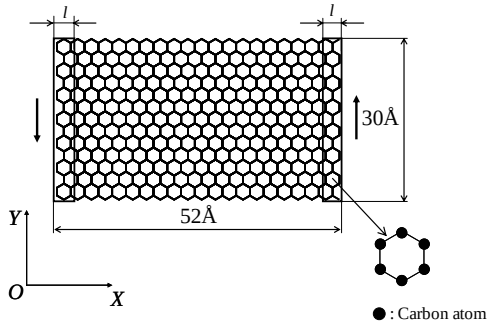

Fig. 1. Configuration of pristine graphene used under shear loading

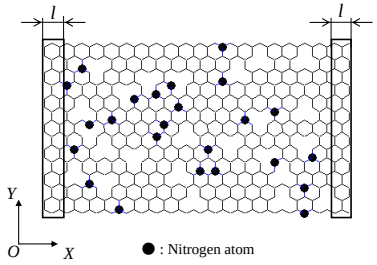

Fig. 2. Configuration of graphene containing vacancies and N-atoms used under shear loading.

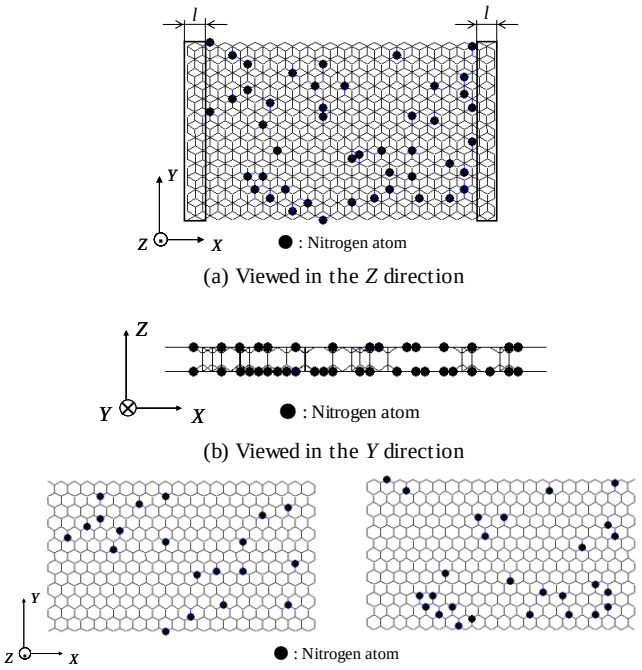

(a) Viewed in the *Z* direction

(b) Viewed in the *Y* direction

(c) Upper layer in the *Z* direction (d) Lower layer in the *Z* direction

Fig. 3. Analysis models for graphene containing interlayer sp^3 carbons and N-atoms

other part enclosed by the boxes as shown in Figs. 1, 2 and 3 is referred to as the boundary zone, in which the atoms are restrained. The thickness l of the boundary zone is $1.5 \times \sqrt{3}a$, where a is the length of C=C bond of graphene.

C. MD simulation

All the MD calculations employ the velocity Verlet method to calculate the time integral of the equations of motion of atoms. The velocities of all atoms are adjusted simultaneously using the velocity scaling method [18] in order to control the temperature of the analysis models by the preset temperature T_{SET}. The mass of carbon atoms, m_C, and the mass of N-atoms, m_N, are 1.9927×10^{-26} kg and 2.3253×10^{-26} kg, respectively. The time step is 0.2 fs.

The atomic stress acting on each atom is calculated to obtain the stress–strain curves during the shear loadings. The atomic stress σ^i_{IJ} which is a component in the J direction in the I-plane is given by calculating the kinetic energies of, the interatomic force acting on, and the volume occupied by atom i, as given in (10):

$$\sigma^i{}_{IJ} = \frac{1}{\Omega^i}\left(m\overline{V^i{}_I V^i{}_J} + \overline{I^i F^i{}_J}\right), \qquad (10)$$

where, Ω^i denotes the volume occupied by atom i, which is referred to as the atomic volume. This volume is calculated by averaging the volume of all atoms in the initial structure of each system. The m can be either m_C or m_N. The $F^i{}_J$ denotes the interatomic force acting on atom i from the neighbouring atoms. The global stress of an analysis model is calculated by averaging over all atoms in each system.

First, the initial positions of the atoms are given such that the analysis model could become identical to the crystal structure of graphene at 300 K. Next, vacancies, nitrogen atoms, and interlayer sp^3 carbons are generated in the analysis model. Then, the atoms of the analysis model are relaxed until the stresses are stabilized for 14,000 MD simulation steps. The atoms in the active zone are relaxed in all the directions. The atoms in the left-hand side boundary zone are relaxed in only the Y direction. The atoms in the right-hand side boundary zone are relaxed in only the X and Y directions. After the atoms are relaxed, constant displacements are applied to the atoms in the boundary zones to simulate shear loading in the Y direction. The atoms in the boundary zones are restrained in all the directions. The atoms in the active zone of the analysis model are relaxed for all the directions for 7,000 MD simulation steps. The shear strain increment $\Delta\gamma_{XY}$ is 0.0023. The shear moduli are obtained from the slopes of the straight lines in the range, where the relation between the stress and strain is linear, and shear strengths are given by the peak of the nominal stress–nominal strain curves.

III. Results and Discussion

A. Shear properties of graphene containing vacancies and nitrogen atoms

MD simulations on shear loadings were performed in order to estimate the shear properties of graphene containing both vacancies and N-atoms. In all the MD calculations, the shear loadings were applied in the armchair direction using the analysis model as shown in Fig. 2. Examples of the stress-strain curves of graphene containing randomly distributed vacancies and N-atoms without adjoining N-atoms are shown in Figs. 4 and 5. The calculated shear strengths and moduli are listed in Tables I and II. On the other hand, the calculated shear strengths and moduli of graphene containing randomly distributed vacancies and N-atoms with two adjoining N-atoms are listed in Tables III and IV.

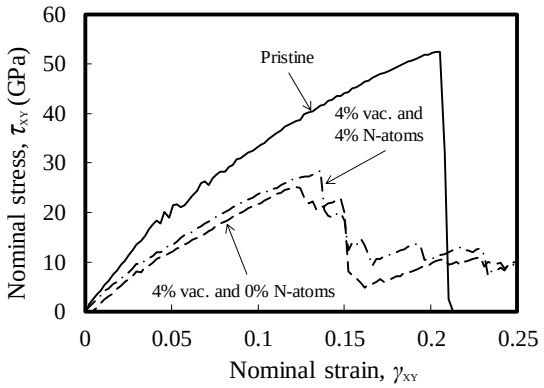

Fig. 4. Stress-strain curves of graphene containing randomly distributed 4 % vacancies and N-atoms without adjoining N-atoms.

TABLE I
Shear Properties of Graphene Containing Randomly Distributed 4 % Vacancies and N- Atoms Without Adjoining N-Atoms

Nitrogen content (%)	Vacancy density (%)	Shear strength (GPa)	Shear modulus (GPa)
0	4	27	290
1	4	26	300
2	4	30	299
4	4	29	301

The relation between the shear properties and N-content is shown in Figs. 6 and 7. Then, the relation between the shear properties and the density of vacancies is shown in Figs. 8 and 9. The error bars denote the range between two values for the results of two cases which have an individual distribution of vacancies or N-atoms.

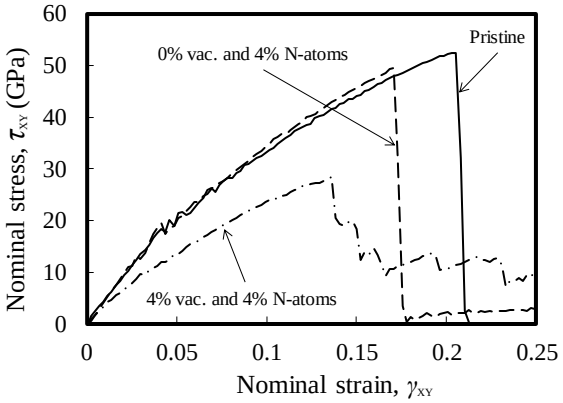

Fig. 5. Stress-strain curves of graphene containing randomly distributed vacancies with each density and 4 % N-atoms without adjoining N-atoms.

TABLE II
SHEAR PROPERTIES OF GRAPHENE CONTAINING RANDOMLY DISTRIBUTED VACANCIES AND 4 % N- ATOMS WITHOUT ADJOINING N-ATOMS

Vacancy density (%)	Nitrogen content (%)	Shear strength (GPa)	Shear modulus (GPa)
0	4	50	466
1	4	39	413
2	4	35	371
4	4	29	301

TABLE III
SHEAR PROPERTIES OF GRAPHENE CONTAINING RANDOMLY DISTRIBUTED 4 % VACANCIES AND N- ATOMS WITH TWO ADJOINING N-ATOMS

Nitrogen content (%)	Vacancy density (%)	Shear strength (GPa)	Shear modulus (GPa)
0	4	27	290
1	4	27	291
2	4	27	295
4	4	27	298

TABLE IV
SHEAR PROPERTIES OF GRAPHENE CONTAINING RANDOMLY DISTRIBUTED VACANCIES AND 4 % N- ATOMS WITH TWO ADJOINING N-ATOMS

Vacancy density (%)	Nitrogen content (%)	Shear strength (GPa)	Shear modulus (GPa)
0	4	42	440
1	4	38	411
2	4	32	374
4	4	27	298

It was found that the shear strength and modulus decrease greatly when graphene contains vacancies at the density of 4 % as shown in Fig. 4. However, the shear strength and the modulus do not change much with a change in the N-content. On the other hand, the shear properties decreased greatly as the density of vacancies increased as shown in Figs. 5, 8, and 9.

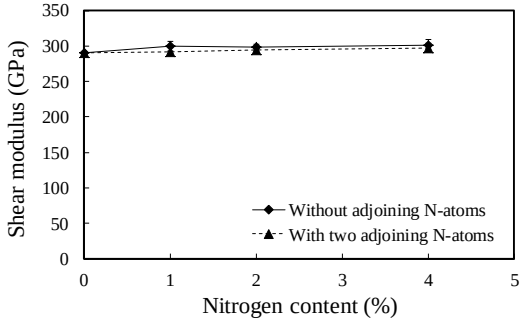

Fig. 6. Shear moduli with N-content in graphene containing N-atoms and 4 % vacancies.

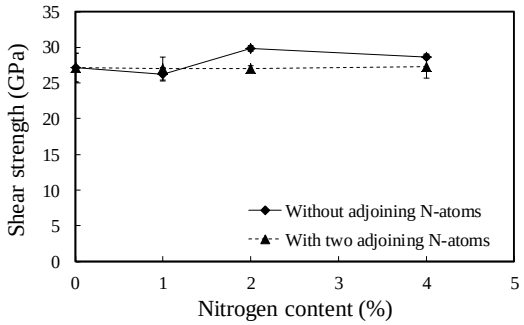

Fig. 7. Shear strengths with N-content in graphene containing N-atoms and 4 % vacancies.

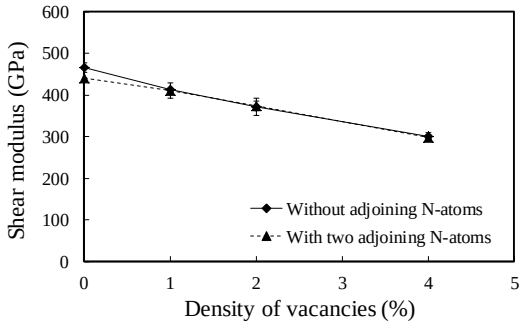

Fig. 8. Shear moduli with density of vacancies in graphene containing vacancies and 4 % N-atoms.

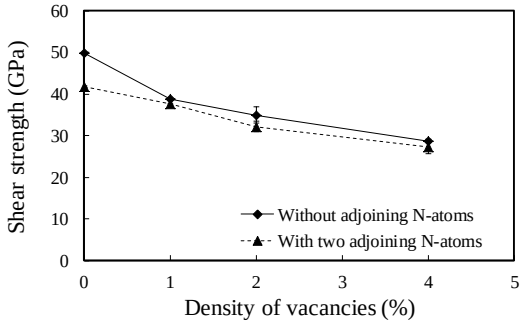

Fig. 9. Shear strengths with density of vacancies in graphene containing vacancies and 4 % N-atoms.

In addition, there is hardly a difference between shear moduli in the two cases, namely, with and without adjoining N-atoms. However the shear strength in the case of containing adjoining N-atoms is slightly smaller than that without adjoining ones.

Snapshots taken during the shear loadings are shown in Figs.10 ,11, and 12. In the case of not containing vacancies (see Figs. 10 ((a-1)–(a-3)), 11 ((a-1)–(a-3)), and 12 ((a-1)–(a-3))), fractures progress in the zigzag direction. In addition, in the case of containing two adjoining N-atoms, a fracture begins at the adjoining N-atoms. On the other hand, in the case of containing vacancies (see Figs. 10 ((b-1)–(b-3)), 11 ((b-1)–(b-3)), and 12 ((b-1)–(b-3))), fractures began around vacancies and progressed in random directions.

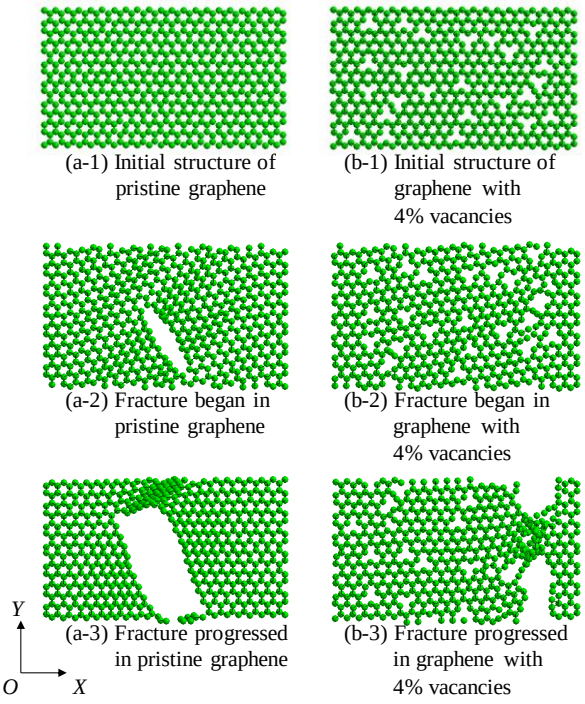

Fig. 10. Atomic structures before shear loading and after fracture for pristine graphene ((a-1)–(a-3)) and graphene with 4 % vacancies ((b-1)–(b-3)).

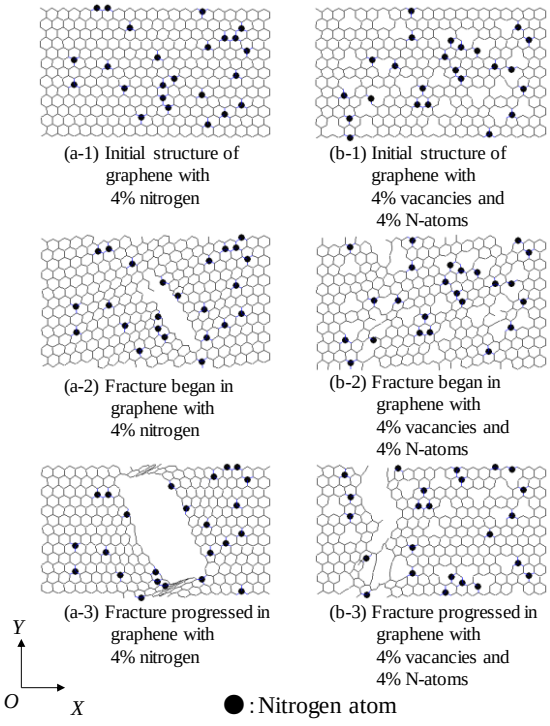

Fig. 11. Atomic structures before shear loading and after fracture for graphene containing 4 % N-atoms without adjoining N-atoms ((a-1)–(a-3)) and graphene containing 4 % vacancies and 4 % N-atoms without adjoining N-atoms ((b-1)–(b-3)).

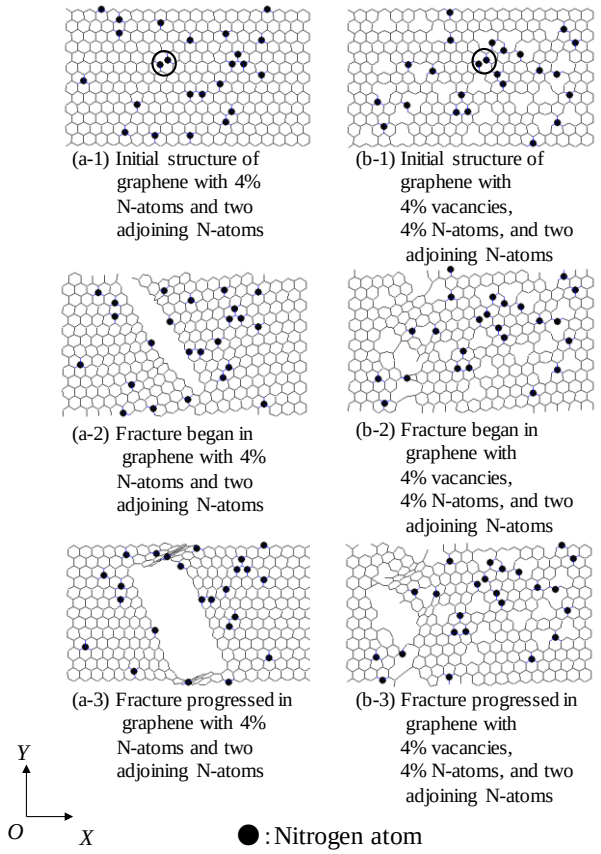

Fig. 12. Atomic structures before shear loading and after fracture for graphene with 4 % N-atoms, and two adjoining N-atoms ((a-1)–(a-3)) and graphene with 4 % vacancies, 4 % N-atoms, and two adjoining N-atoms ((b-1)–(b-3)).

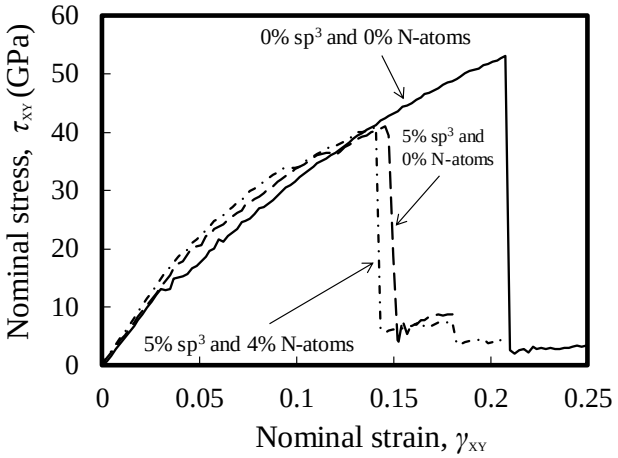

Fig. 13. Stress-strain curves of bilayer graphene containing randomly distributed 5 % sp^3 carbons and N-atoms with each density.

TABLE V
SHEAR PROPERTIES OF GRAPHENE CONTAINING RANDOMLY DISTRIBUTED 5 % Sp^3 CARBONS AND N- ATOMS

Nitrogen content (%)	Sp^3-carbons density (%)	Shear strength (GPa)	Shear modulus (GPa)
0	0	53	440
0	5	41	437
1	5	40	454
4	5	41	492

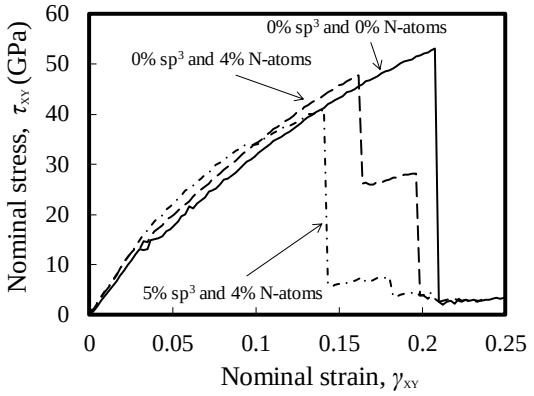

Fig. 14. Stress-strain curves of bilayer graphene containing randomly distributed sp^3 carbons with each density and 4 % N-atoms.

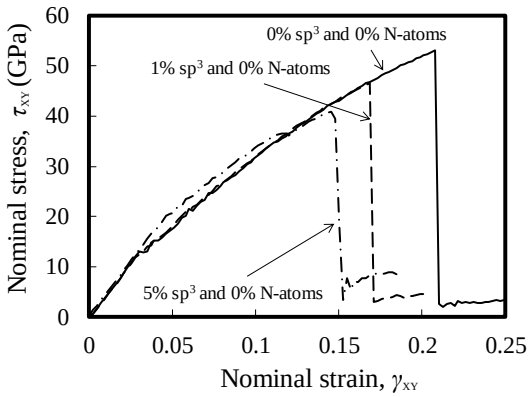

Fig. 15. Stress-strain curves of bilayer graphene containing randomly distributed sp^3 carbons with each density and 0 % N-atoms.

B. Shear properties of bilayer graphene containing interlayer sp^3 carbons and nitrogen atoms

MD simulations on shear loadings of bilayer graphene containing interlayer sp^3 carbons and N-atoms were performed in order to investigate the effect of sp^3 carbons and N-atoms on the shear properties of graphene. Examples of the stress-strain curves of bilayer graphene containing randomly distributed sp^3 carbons and N-atoms are shown in Figs. 13, 14, and 15. The calculated shear strengths and moduli are listed in Tables V and VI. The relation between the shear properties and N-content is shown in Fig. 16. Then, the relation between the shear properties and density of sp^3 carbons is shown in Fig. 17.

It was found that the shear strength decreases greatly when bilayer graphene contains sp^3 carbons at the density of 5 % as shown in Fig. 13.

However, the shear strength and modulus do not change much with a change in the N-content as shown in Fig. 16.

On the other hand, the shear strength decreases slightly as the density of sp^3 carbons increases as shown in Figs. 15 and 17. The decline in shear strength is around 15 % when the density of sp^3 carbons is 5 %. The percentage of decline is almost same as that obtained in the experiment (～14 %) [2]. Moreover, the shear modulus maintains a almost constant value even if the density of sp^3 carbons is large, and also is the almost same as the experimental result.

Snapshots taken during the shear loadings of bilayer graphene with 5 % sp^3 carbons and 4 % N-atoms are shown in Fig. 18. The case of pristine bilayer graphene is also shown for a reference. In the case of pristine bilayer graphene ((a-1)–(a-3)), a fracture begins at the center of each layer and progress in the zigzag direction. On the other hand, in the case of bilayer graphene with sp^3 carbons and N-atoms ((b-1)–(b-3)), a fracture begins at the other point.

TABLE VI
SHEAR PROPERTIES OF GRAPHENE CONTAINING RANDOMLY DISTRIBUTED Sp^3 CARBONS AND 4 % N- ATOMS

Nitrogen content (%)	Sp^3-carbon density (%)	Shear strength (GPa)	Shear modulus (GPa)
0	0	53	440
0	1	47	427
0	5	41	437
4	0	48	472
4	1	48	481
4	5	41	492

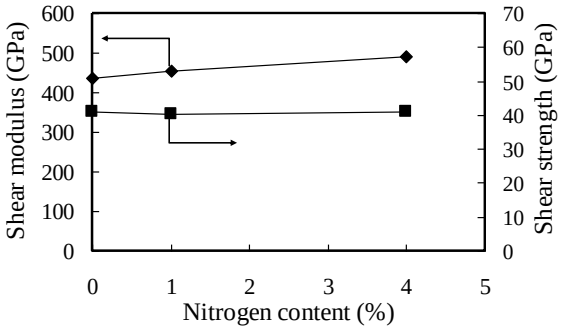

Fig. 16. Shear modulus and strength with N-content in graphene containing N-atoms and 5 % sp^3 carbons.

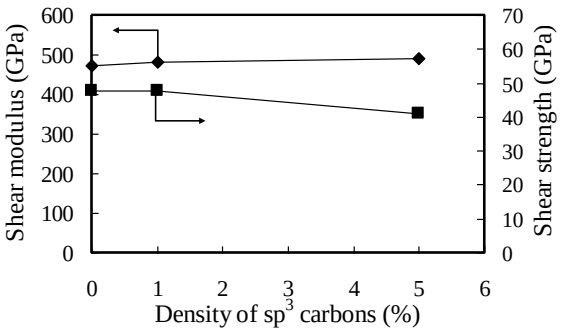

Fig. 17. Shear modulus and strength with the density of sp^3 carbons in graphene containing sp^3 carbons and 4 % N-atoms.

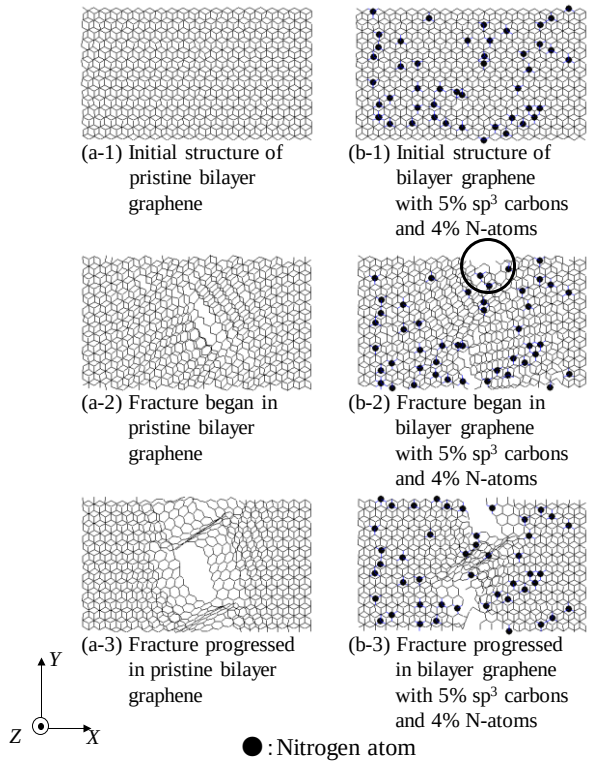

Fig. 18. Atomic structures before shear loading and after fracture for pristine bilayer graphene ((a-1)–(a-3)) and bilayer graphene with 5 % sp^3 carbons and 4 % N-atoms ((b-1)–(b-3)).

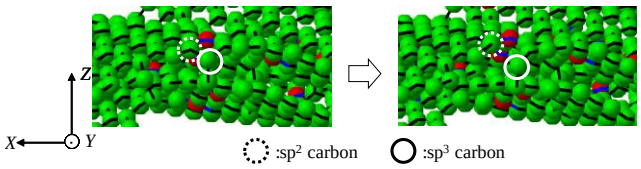

(a) Before cleavage (b) After cleavage

Fig. 19. Cleavage of the bond between sp^2 and sp^3 carbons

The enlargement of the area circled in Fig. 19 (b-2) is shown in Fig. 19. The atoms enclosed by blue and red circles denote sp^2 and sp^3 carbons, respectively. It was found that the fracture begin because of the cleavage of the bond between sp^2 and sp^3 carbons

IV. Conclusion

We investigated the shear properties of graphene containing point defects, such as vacancies, nitrogen atoms, and interlayer sp^3 carbons using the MD simulations. It was found that the effect on the shear strength of graphene increases in the order of nitrogen atom, interlayer sp^3 carbon, and vacancy unless these defects cluster in graphene. Therefore, the fractures begin around vacancies in graphene containing randomly distributed vacancies and nitrogen atoms. The shear strength of graphene containing adjoining N-atoms is smaller than that without adjoining ones.

References

[1] P. A. Thrower, "The Study of Defects in Graphite by Transmission Electron Microscopy," *Chemistry and Physics of Carbon*, vol.5, pp. 217, 1969.

[2] A. Zandiatashbar, G-H. Lee, S. J. An, S. Lee, N. Mathew, M. Terrones, T. Hayashi, C. R. Picu, J. Hone, and N. Koratkar, "Effect of Defects on the Intrinsic Strength and Stiffness of Graphene," *Nature Communications*, vol. 5, Jan., 2014.

[3] V. Serin, R. Fourmeaux, Y. Kihn, and J. Sevely, "Nitrogen distribution in high tensile strength carbon fibres," Carbon, vol. 28, pp. 573–578, 1990.

[4] A. Hashimoto, K. Suenaga, A. Gloter, K. Urita, and S. Iijima, "Direct Evidence for Atomic Defects in Graphene Layers," *Nature*,vol.430, pp.870-873, Aug., 2004.

[5] A. Capasso, E. Placidi, H. F. Zhan, E. Perfetto, J. M. Bell, Y. T. Gu, and N. Motta, "Graphene ripples generated by grain boundaries in highly ordered pyrolytic graphite," *Carbon*, vol.68, pp. 330–336, Mar., 2014.

[6] A. Ito, S. Okamoto, "Molecular Dynamics Analysis on Effects of Vacancies upon Mechanical Properties of Graphene and Graphite," *Engineering Letters*, vol.20, pp.271-278, Aug., 2012.

[7] L. Shen and Z. Chen, "An investigation of grain size and nitrogen-doping effects on the mechanical properties of ultrananocrystalline diamond films," *International Journal of Solids and Structures*, vol. 44, pp. 3379–3392, May, 2007.

[8] S. Okamoto and A. Ito, "Effects of Nitrogen Atoms on Mechanical Properties of Graphene by Molecular Dynamics Simulations," *Engineering Letters*, vol.20, pp. 169–175, May, 2012.

[9] Y.Y. Zhang, C.M. Wang, Y. Cheng, Y. Xiang, "Mechanical Properties of Bilayer Graphene Sheets Coupled by Sp^3 Bonding," *Carbon*, vol.49, pp. 4511–4517, Jun., 2011.

[10] K. Min and N. R. Aluru, " Mechanical properties of graphene under shear deformation," *Applied Physics Letters*, vol.98, pp. 013113-1–013113-3, Jan., 2011.

[11] A. Ito and S. Okamoto, "Effect of Point Defects on Shear Properties of Graphene Using Molecular Dynamics Simulations," *Lecture Notes in Engineering and Computer Science: Proceedings of The International MultiConference of Engineering and Computer Scientists 2014 Vol II*, IMECS 2014, 12-14 Mar., 2014, Hong Kong, pp.886-891.

[12] D. W. Brenner, O. A. Shenderova, J. A. Harrison, S. J. Stuart, B. Ni, and S. B. Sinnott, "A second-generation reactive empirical bond order (REBO) potential energy expression for hydrocarbons," *Journal of Physics*: *Condensed Matter*, vol. 14, pp. 783–802, Jan., 2002.

[13] J. Tersoff, "Modeling solid-state chemistry: interatomic potentials for multicomponent systems," *Physical Review B*, vol. 39, no. 8, pp.5566–5568, Mar., 1989.

[14] J. Tersoff, "Structural properties of amorphous silicon nitride," *Physical Review B*, vol. 58, no. 13, pp. 8323–8328, Oct., 1998.

[15] S. J. Stuart, A. B. Tutein and J. A. Harrison, "A reactive potential for hydrocarbons with intermolecular interactions," *Journal of Chemical Physics*, vol. 112, no. 14, pp. 6472-6486, Jan., 2000.

[16] W. Ruland, "X-ray studies on the structure of graphitic carbons," *Acta Crystallographica*, vol.18, pp. 992–996, Jun. 1965.

[17] D. J. Johnson, Handbook of polymer-fibre composites, Longman Publishing Group (1994) 24-29.

[18] L. V. Woodcock, "Isothermal molecular dynamics calculations for liquid salts," *Chemical Physics Letters*, vol. 10, pp. 257–261, Aug., 1971.